



# Electrochemical method for isolation of chitinous 3D scaffolds from cultivated *Aplysina aerophoba* marine demosponge and its biomimetic application

Krzysztof Nowacki<sup>1</sup> · Izabela Stępnia<sup>1</sup> · Tomasz Machałowski<sup>2,3</sup> · Marcin Wysokowski<sup>2,3</sup> · Iaroslav Petrenko<sup>3</sup> · Christoph Schimpf<sup>4</sup> · David Rafaja<sup>4</sup> · Enrico Langer<sup>5</sup> · Andreas Richter<sup>5</sup> · Jerzy Ziętek<sup>6</sup> · Snežana Pantović<sup>7</sup> · Alona Voronkina<sup>8</sup> · Valentine Kovalchuk<sup>9</sup> · Viatcheslav Ivanenko<sup>10,11</sup> · Yuliya Khrunyk<sup>12,13</sup> · Roberta Galli<sup>14</sup> · Yvonne Joseph<sup>3</sup> · Michael Gelinsky<sup>15</sup> · Teofil Jesionowski<sup>2</sup> · Hermann Ehrlich<sup>3,16</sup>

Received: 16 March 2020 / Accepted: 7 April 2020  
© The Author(s) 2020

## Abstract

Three-dimensional (3D) biopolymer-based scaffolds including chitinous matrices have been widely used for tissue engineering, regenerative medicine and other modern interdisciplinary fields including extreme biomimetics. In this study, we introduce a novel, electrochemically assisted method for 3D chitin scaffolds isolation from the cultivated marine demosponge *Aplysina aerophoba* which consists of three main steps: (1) decellularization, (2) decalcification and (3) main deproteinization along with desilicification and depigmentation. For the first time, the obtained electrochemically isolated 3D chitinous scaffolds have been further biomineralized ex vivo using hemolymph of *Cornu aspersum* edible snail aimed to generate calcium carbonates-based layered biomimetic scaffolds. The analysis of prior to, during and post-electrochemical isolation samples as well as samples treated with molluscan hemolymph was conducted employing analytical techniques such as SEM, XRD, ATR–FTIR and Raman spectroscopy. Finally, the use of described method for chitin isolation combined with biomineralization ex vivo resulted in the formation of crystalline (calcite) calcium carbonate-based deposits on the surface of chitinous scaffolds, which could serve as promising biomaterials for the wide range of biomedical, environmental and biomimetic applications.

**Keywords** Chitin · Scaffolds · Electrolysis · Biomineralization · Biomimetics · Hemolymph · Marine sponges · *Aplysina aerophoba*

## 1 Introduction

In recent decades, the synthesis and application of 3D biopolymer-based scaffolds represent one of the new trends in environmental science and technology. Owing to their ability to mimic the patterns of natural structures, excellent biocompatibility, high biodegradability and non-toxicity 3D scaffolds of natural origin find increasing applications in medicine, biotechnology and various interdisciplinary fields including tissue engineering, biomimetics, biocatalysis,

adsorption techniques and wastewater treatment [1–10]. Highly versatile and promising biopolymers such as cellulose, chitin, collagen and their derivatives are more and more frequently used in modern technology [11–16].

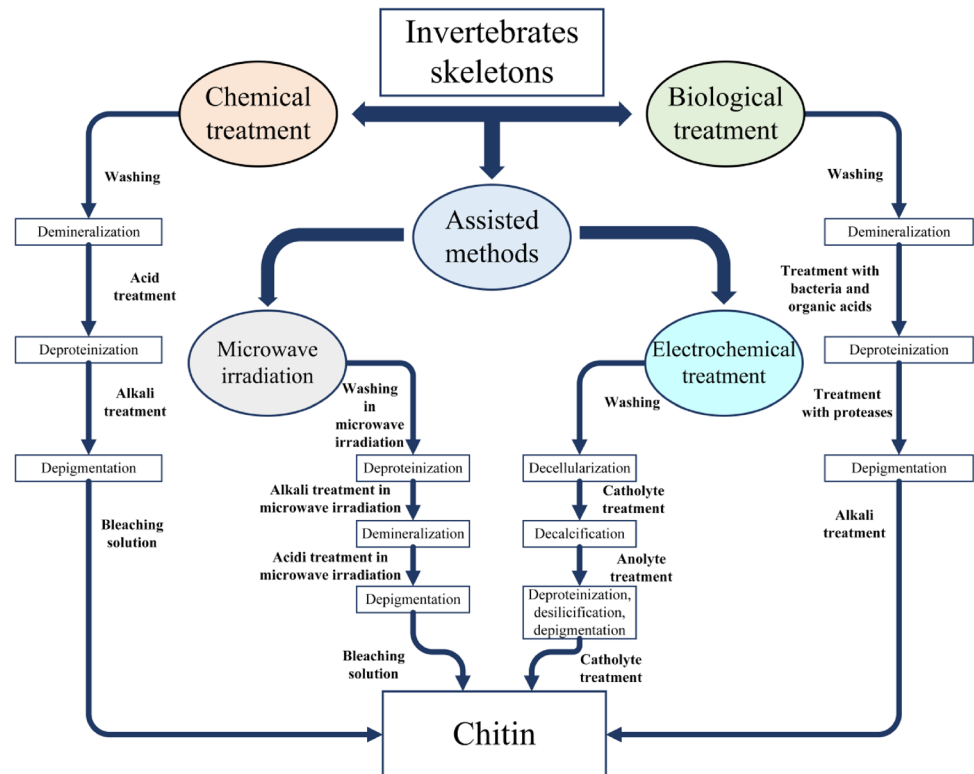
Chitin is one of the most abundant polysaccharides of natural origin, obtained mainly from crustaceans, although it can be found in representatives of diatoms, sponges, mollusks, tubeworms, insects and arachnids [17–22]. This biopolymer is composed of  $\beta$ -(1,4)-*N*-acetyl-D-glucosamine units and plays a crucial role in the formation of both soft and mineralized skeletal structures in invertebrates requiring rigidity and mechanical strength [23, 24]. Usually, chitin as a source of industrially produced chitosan is isolated by two main types of extraction process: chemical and biological methods. The schematic view showing principal steps of each method is represented in Fig. 1 [25, 26]. In brief, industrial chemical

✉ Krzysztof Nowacki  
krzysztof.j.nowacki@doctorate.put.poznan.pl

✉ Izabela Stępnia<sup>1</sup>  
izabela.stepniak@put.poznan.pl

Extended author information available on the last page of the article

**Fig. 1** Schematic diagram showing the isolation of chitin (for details see Refs. [25, 26])



treatment involves three major steps: deproteinization, demineralization and depigmentation. Protein hydrolysis occurring in the first step is carried out using alkali solutions such as NaOH or KOH. In this stage of the isolation process, the efficiency mostly depends on the concentration of a base, temperature and duration of treatment [27]. It should be also noted that for proper deproteinization of chitin precursor a great excess of the alkali solution must be used. The second step is usually completed by treating the source of chitin with acid solution ( $\text{CH}_3\text{COOH}$  or HCl) to ensure elimination of calcium carbonates. In order to isolate chitinous skeleton, deproteinization and demineralization steps are often repeated. The final treatment step, depigmentation, is performed by adding highly reactive oxidizing agents such as hydrogen peroxide. A major drawback of the chemical isolation is caused by the use of hazardous to the environmental extraction agents. Moreover, these chemicals are used in great excess, generating effluents that must be neutralized prior to disposal [28–30]. To prevent this negative environmental effect, the biological/enzymatic treatment was developed as an alternative method of chitin isolation [31–33]. According to this method, chemical extraction steps are substituted by the action of microorganisms and enzymes (see Fig. 1). Though requiring more time, such biological treatment results in the isolation of chitin with a better preserved spatial structure [34]. Notwithstanding, in order to increase the efficiency of biological method and reduce the

environmental impact of chemical process, the novel and modified methods of chitin isolation have been developed in recent time [35–38].

Marine demosponges have been recognized as a novel source of naturally prefabricated 3D matrices and remain to be the subject of intense research with respect to designing of effective approaches to extract ready-to-use chitinous scaffolds [38–40]. For this purpose, a well-established chemical method was developed and since this treatment involves acidic and alkali extraction steps that are cyclically repeated, the process duration often exceeds 72 h [41, 42]. Therefore, this method is often modified in order to reduce treatment time and the amount of chemicals that are used. Recently reported methods of chitin extraction are mostly focused on the use of microwave irradiation as accelerating factor [43, 44].

The only proposed approach including electrochemical treatment of a chitin precursor was described previously by Prof. Kuprina group [45–49]. The principle of this method is based on the electrolysis of diluted NaCl aqueous solution to ensure acidic and alkali treatment of crustacean's *Gammarus pulex* (Linnaeus, 1758) biomass [49].

Electrolysis is a well-known electrochemical process that is thermodynamically forced by the flow of direct electric current from an external source [50–52]. For this process to function, a specific electrolytic cell (electrolyzer) must be constructed: Briefly, the apparatus is composed from two chambers and two symmetrical polarizable electrodes

made from chemically inert materials with high surface area. Usually both electrodes are dipped in liquid electrolyte and separated with an ion exchange membrane (cation, anion or bipolar) [53–62]. Electrolysis of aqueous salts solutions (NaCl or Na<sub>2</sub>SO<sub>4</sub>) in ion exchange membrane electrolyzers is a relatively easy method to produce alkali and acids. One of the most popular processes in industry is electrolysis of Na<sub>2</sub>SO<sub>4</sub> aqueous solution in a cation exchange membrane (CEM) electrolyzer [60]. The basic principle of this process is shown in Fig. 2 [61].

In brief, the conversion of Na<sub>2</sub>SO<sub>4</sub> to NaOH and H<sub>2</sub>SO<sub>4</sub> can be separated in two steps: (1) electrochemical decomposition of water particles and (2) separation of sodium cations and sulfate anions [58]. The first step occurs on the anode surface:



and on the cathode surface:



These redox reactions result in excess of H<sup>+</sup> ions in electrolyte solution in anode chamber (anolyte) and OH<sup>-</sup> ions in cathode chamber (catholyte). Owing to this phenomenon, boosted by synergic effect of the separation of sodium cations and sulfate anions on the CEM membrane, it is possible to establish and change pH in each part of electrolyzer by applying specific potential conditions.

Electrolysis has never been used for the isolation of sponge chitin. In this study, for the first time, we applied concentrated Na<sub>2</sub>SO<sub>4</sub> aqueous solution as electrolyte for a novel electrochemical method which was designed by combining well-known chemical treatment of chitin-based skeleton of cultivated under marine farming conditions [63] *Aplysina aerophoba* (Nardo 1833) marine demosponges with in situ electrolysis. Finally, we used electrochemically isolated 3D chitinous scaffolds for their biomimetic biomineralization ex vivo using hemolymph of industrially cultivated edible snail *Cornu aspersum* with the aim of developing calcium carbonate based scaffolds potentially applicable for environmental remediation.

## 2 Materials and methods

### 2.1 Biological samples and chemicals

#### 2.1.1 *Aplysina aerophoba* demosponges

Selected specimens of cultivated *A. aerophoba* (Nardo, 1833) marine demosponges [63] in the form of air-dried material (see Fig. 3) were purchased from BromMarin GmbH, Freiberg, Germany. Sodium sulfate [≥99.7% (VWR, Dresden, Germany)] was used for the preparation of aqueous electrolyte solution. All aqueous solutions were prepared with distilled water.

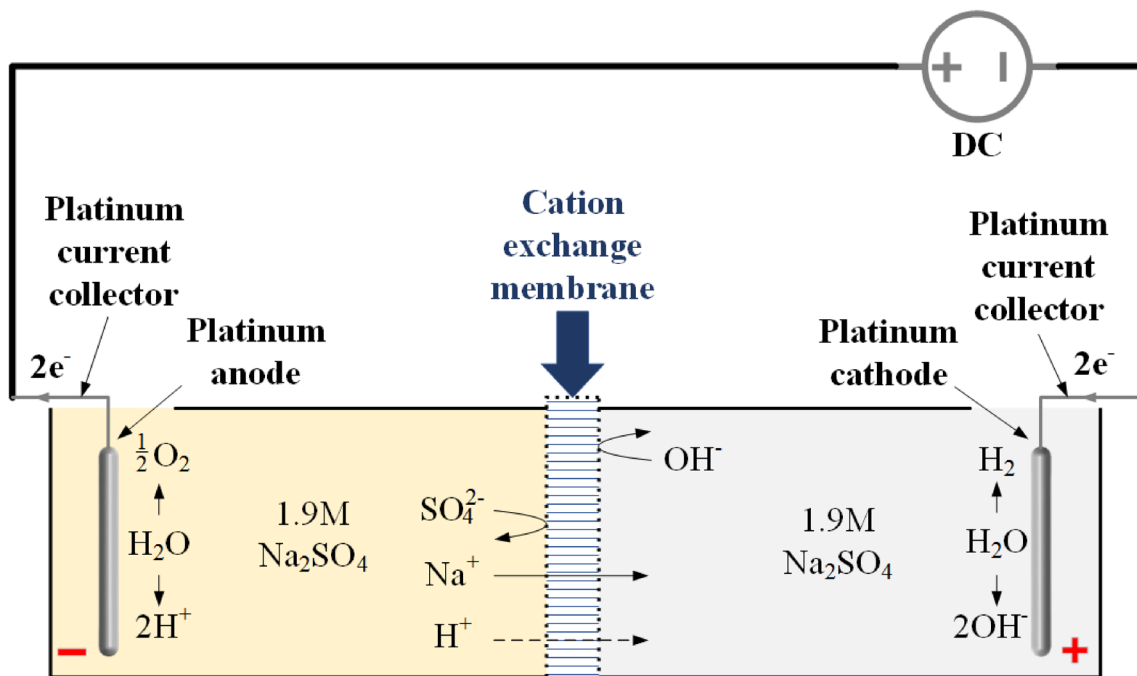


**Fig. 2** Schematic illustration of the electrolysis cell assembled in this study and a general principle of Na<sub>2</sub>SO<sub>4</sub> aqueous solution electrolysis [61]

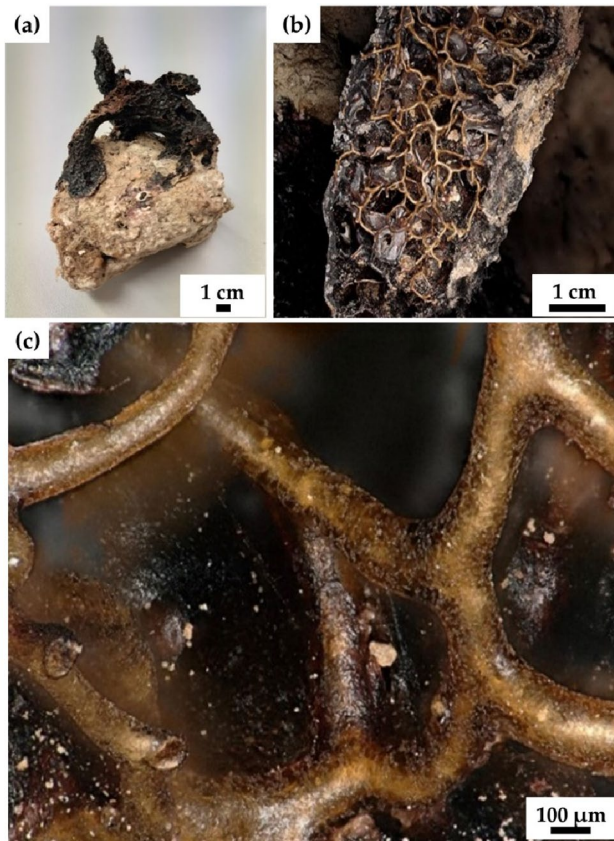


**Fig. 3** Fragment of *A. aerophoba* demosponge from the marine ranching facility in Kotor Bay, Montenegro (a, b). Mineralized and pigmented skeletal fibers (c) remain to be rigid after drying on air at 28 °C

### 2.1.2 *Cornu aspersum* snails

One-year-old snails *C. aspersum* were obtained from a commercial heliculture farm from the central part of Poland (Snails Breeder—Hodowla Ślimaków, Małaszyce, Poland). Snails were maintained in a special glass aquarium at room temperature. As food, lettuce, carrots and apples were traditionally used. Additionally, cuttlebone of *Sepia officinalis* cuttlefish was given to snails as calcium carbonate enrichment ( $\text{CaCO}_3$ ) in the diet. The snails were kept moist throughout the experimental period with wet humus. Animal rights statement is not required.

## 2.2 Non-lethal hemolymph sampling procedure

For hemolymph collection, the modified non-lethal intravital method described previously [64, 65] was used. The shell surface of the selected *C. aspersum* snail was cleaned by 70% ethanol. After that, a piece of shell was removed and 3 h later about 0.5 ml of hemolymph was isolated from an individual of *C. aspersum* by main vessel puncture using

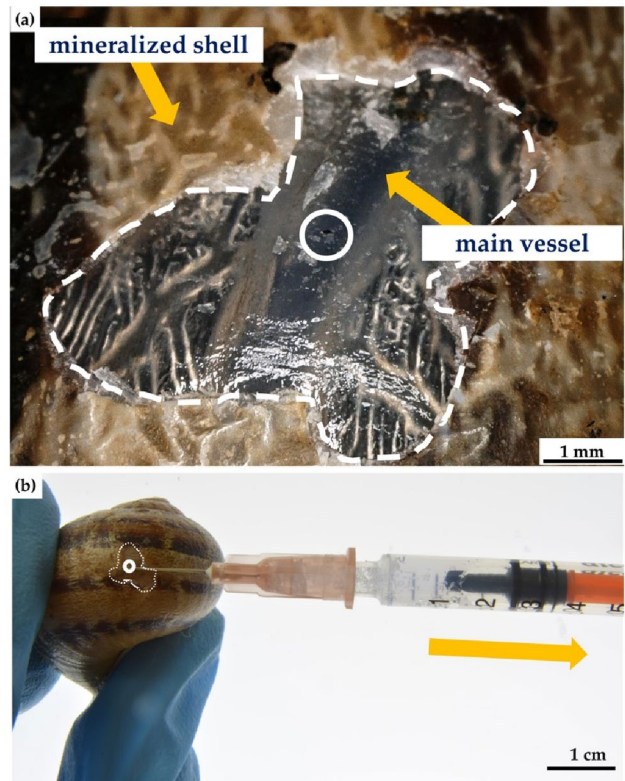


**Fig. 4** Non-lethal isolation of the hemolymph from *C. aspersum* snail. Initially, a small fragment of the shell (around 5 mm×5 mm) was carefully removed using scalpel with the aim to obtain an access to the main vessel (a). Common view of the procedure of non-lethal hemolymph aspiration using sterile syringe and needle (b)

a sterile 1 ml syringe and needle of 0.45 mm in diameter [64, 65] (see Fig. 4). Twelve hours post-isolation, an organic film was observed in the site of the removed shell fragment, which was fully mineralized within the next few days. During the next four months after the procedure, the snails used in this study did not show any visible changes neither in their physiology nor in behavior.

## 2.3 Electrolytic cell setup

Schematic diagram of the experimental setup for the electrochemically assisted isolation of chitin is depicted in Fig. 2. The CEM (cation exchange membrane) electrolyzer consisted of two cylindrical poly(propylene) chambers (50 ml each) separated by a cellulose membrane made from filter paper ( $75 \text{ g cm}^{-2}$  (ChemLand, Stargard, Poland)) and sealed with parafilm (Bemis Company Inc., Neenah, USA). Electrodes (cathode and anode) were made of platinum sheets (effective area:  $2.2 \text{ cm}^2$ ). Distance between both electrodes was about 10.0 cm and they were connected with DC power supply [VoltCraft PS2043D (Conrad Electronic Group, Hirschau, Germany)] by platinum wire current collectors.

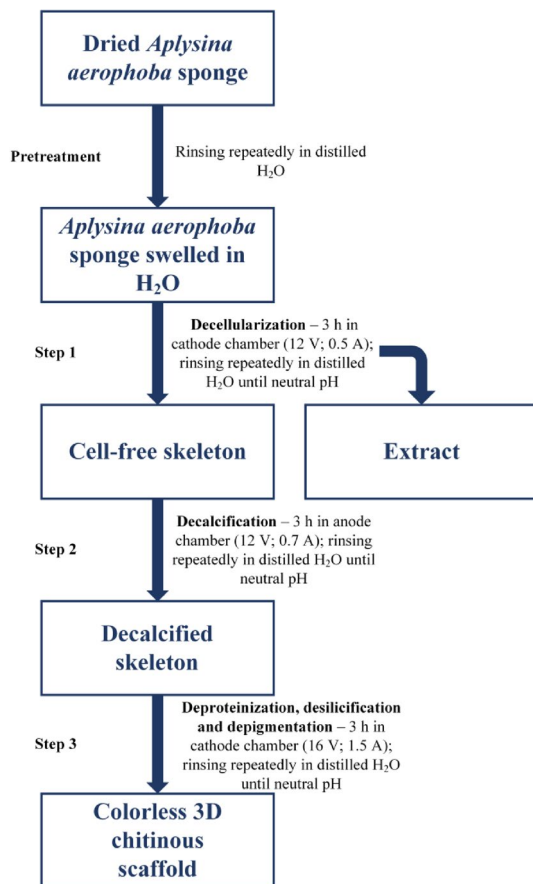


**Fig. 5** Schematic view of the electrochemically assisted isolation of chitin scaffold from *A. aerophoba*

1.9 M sodium sulfate aqueous solution with an initial temperature of 40 °C was utilized as anolyte as well as catholyte.

## 2.4 Electrochemically assisted isolation of sponge chitin

The isolation of chitin scaffold from *A. aerophoba* was performed by novel electrochemically assisted method (see Fig. 5) proposed in this study. In the pretreatment step, 0.2 g *A. aerophoba* sample was rinsed repeatedly with distilled water for 24 h (25 °C) in order to remove water-soluble salts and various major impurities. Water-swelled sample, free from impurities and with partially lysed cells, was ready for treatment in electrolyzer. It should be noted that after each step the sample was extensively washed and stirred in distilled water till neutral pH. Also, the initial concentration of electrolyte ( $\text{Na}_2\text{SO}_4$ ) for every step was 1.9 mol  $\text{l}^{-1}$  and start temperature for both anolyte and catholyte was 40 °C.

Electrochemical treatment was performed in three main steps (see Fig. 6).

*Step 1* Decellularization (predeproteinization) was carried out in the cathode chamber for 3 h (12 V; 0.5 A;

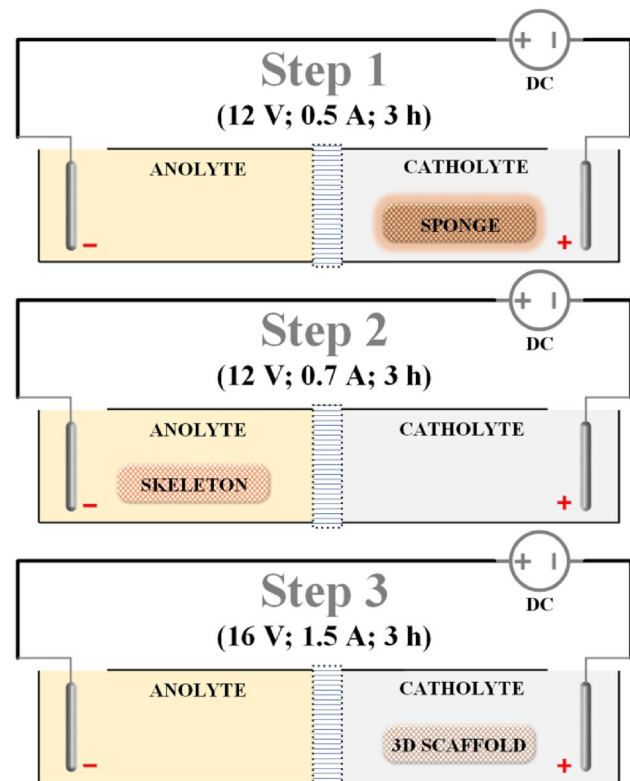


**Fig. 6** Experimental setup for all steps of the electrochemically assisted isolation of sponge chitin in the form of 3D scaffold

50 °C). High pH of the catholyte (up to 12.0) caused a complete lysis of preswelled cells and a partial degradation of lipids and proteins which resulted in the removal of soft tissues. Post-treated sample was composed of deep brown cell-free skeleton.

*Step 2* Decalcification (demineralization) was performed in the anode chamber for 3 h (12 V; 0.7 A; 50 °C). Low pH (down to 1.5) along with free access of the anolyte solution to the sponge skeleton resulted in the dissolution of calcium and magnesium carbonate, acid-soluble pigments and proteins. Post-treated sample was in form of a light yellow cell-free skeleton.

*Step 3* Main deproteinization, desilicification and depigmentation were conducted in the cathode chamber for 3 h (16 V; 1.5 A; 60 °C). Extremely high pH (up to 12.5) of the catholyte caused by increased electrolysis current was used to completely remove pigments and residual proteins from the chitinous matrix. Post-treated sample presented a colorless scaffold. After treatment in the electrolyzer, the sample was once more extensively rinsed with distilled water until neutral pH and stored in ethanol absolute (4 °C).

## 2.5 Biom mineralization ex vivo of electrochemically isolated *A. aerophoba* dem osponge chitinous scaffolds

A square fragment (10 × 10 mm) of selected chitinous scaffold was immersed in hemolymph of *C. aspersum* for one hour and then placed on a sterile slide until completely dried at room temperature. This procedure was repeated for five times. The described technique aimed to simulate biom mineralization of organic matrix by living snail under natural conditions via mimicking of physicochemical effects reported for shell regeneration of terrestrial snails previously [66–68]. Obtained in this way, mineral phases deposited on chitinous matrix were characterized as represented below.

## 2.6 Short-term cultivation of hemocytes on chitinous matrix

For short-term cultivation of hemocytes about 0.5 ml of the *C. aspersum* hemolymph was isolated using the method described above and placed in 2-ml Eppendorf vessel. Selected fragment of electrochemically isolated chitinous matrix as represented in Fig. 7n was immersed in the hemolymph at room temperature for 24 h. To prevent possible bacterial contamination, streptomycin [100 µg ml<sup>-1</sup> (Merck, Darmstadt, Germany)] and penicillin [60 µg ml<sup>-1</sup> (Merck, Darmstadt, Germany)] were used [69].

## 2.7 Characterization of obtained materials

### 2.7.1 Photography and figures

Photographs and macroscopic images were performed by Nikon D-7100 camera with Nikon AF-S DX 18–105 mm f/3.5–5.6G and Nikon AF-S VR Micro-Nikkor 105 mm f/2.8G IF-ED objective lenses. Figures were prepared using the GNU Image Manipulation Program GIMP and the Microsoft Office tool PowerPoint 2016.

### 2.7.2 Digital, light and fluorescence microscopy

The samples were observed using advanced imaging and measurement system consisting of Keyence VHX-6000 digital optical microscope and the swing-head zoom lenses VH-Z20R (magnification up to 200×) and VH-Z100UR (magnification up to 1000×) (Keyence, Osaka, Japan). The light and fluorescence microscopy mode was performed by Keyence BZ-9000 (Keyence, Osaka, Japan) microscope. Calcite mineral standard has been purchased from International Institute of Biomineralogy (INTIB GmbH, Freiberg, Germany).

### 2.7.3 Eosin and methylene blue staining

Hemavet (Kolchem, Łódź, Poland), the combination of eosin and methylene blue dyes, was used. Previously, this stain was successfully used for hemocyte detection and characterization [70, 71]. Hemolymph cell monolayers (HCMs) were prepared by spreading the drop of hemolymph on sterile glass slide and drying it at ambient temperature. Staining was also used to detect hemocytes settled on chitinous scaffold (see Fig. 9).

### 2.7.4 Alizarin Red S staining

Ex vivo mineralized chitinous scaffolds were stained with Alizarin Red S (Sigma-Aldrich, Taufkirchen, Germany) and compared with that of native *A. aerophoba* chitin as isolated. For the staining procedure 40 mM of Alizarin Red S (pH 8.3) was used for staining of the samples during 30 min at room temperature (for details see [72]). Stained samples were washed with distilled water for ten times to eliminate the unattached Alizarin Red S as well as mineral particles which were not tightly attached to the surface of chitin fibers. Calcium deposits were detected as orange–red color microagglomerates employing digital microscopy.

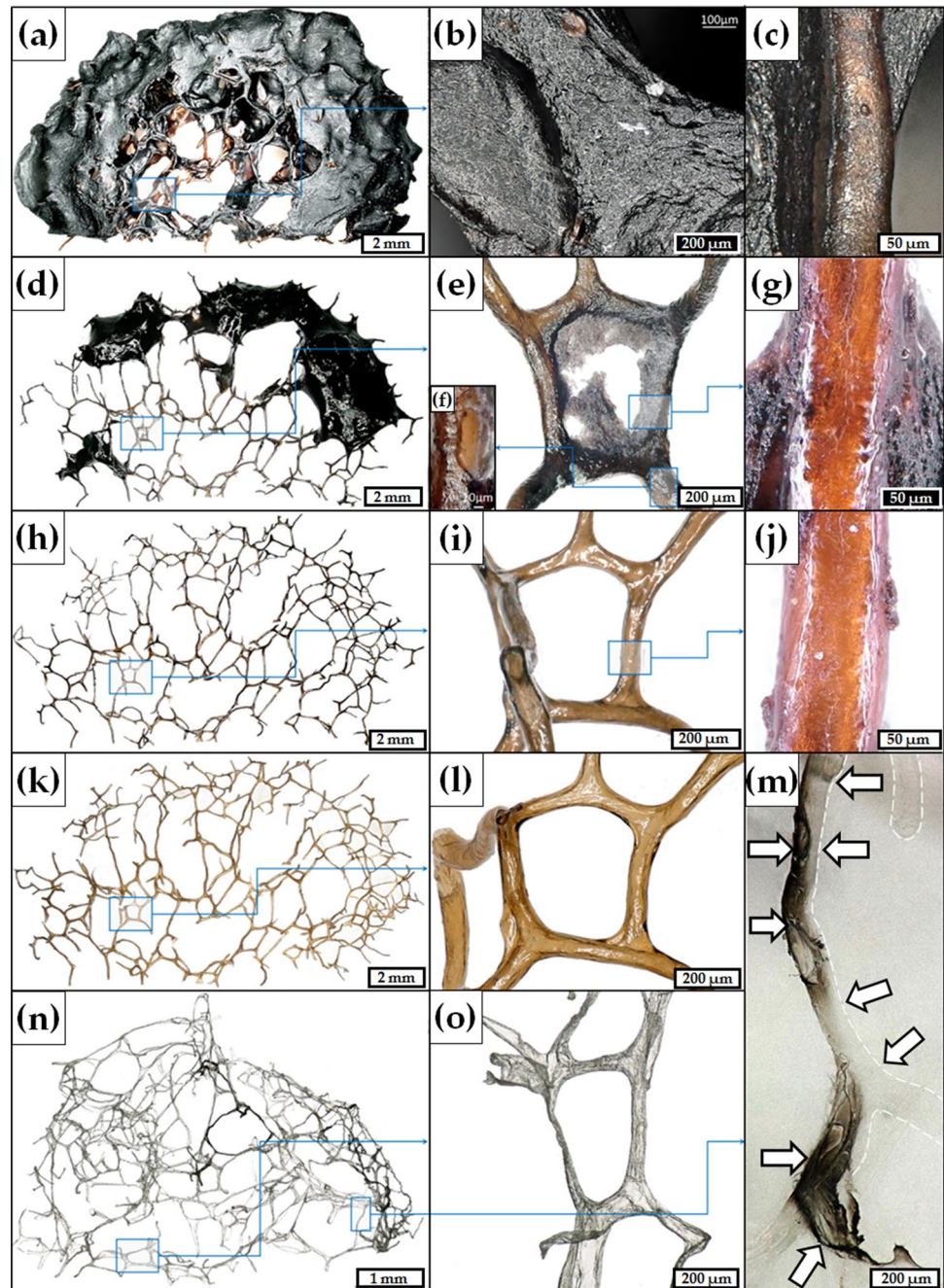
### 2.7.5 ATR–FTIR spectroscopy

Infrared spectroscopy techniques were used for the qualitative characterization of obtained mineralized scaffolds as well as pure chitin isolated from *A. aerophoba*. The presence of expected functional group was confirmed by ATR–FTIR (attenuated total reflectance–Fourier transform infrared spectroscopy) and verified using Nicolet 210c spectrometer (Thermo Scientific, Waltham, USA). The investigation was performed over a wave number range of 1900–500 cm<sup>-1</sup> (resolution of 0.5 cm<sup>-1</sup>).

### 2.7.6 Raman spectroscopy

Raman spectra were recorded using a Raman spectrometer RamanRxn1 (Kaiser Optical Systems Inc., Ann Arbor, USA) coupled to a light microscope DM2500 P (Leica Microsystems GmbH, Wetzlar, Germany). The excitation of Raman scattering was obtained with a diode laser emitting at a wavelength of 785 nm, propagated to the microscope with a 100 µm optical fiber and focused on the samples by means of a 50×/0.75 microscope objective, leading to a focal spot of about 20 µm with a power of 170 mW. The Raman signal was collected in reflection configuration and sent to the f/1.8 holographic imaging spectrograph by using 62.5 µm core optical fiber. The spectral resolution in the range of 150–3250 cm<sup>-1</sup> was 4 cm<sup>-1</sup>. Raman spectra were punctually recorded, using integration time of 1 s and averaging

**Fig. 7** *A. aerophoba* sample prior to (a–c) and at different stages of electrochemically assisted isolation of chitinous 3D scaffolds: 1.5 h (d–g) and 3 h (h–j) starting from the first catholyte treatment; 3 h following anolyte treatment (k, l) and 3 h post-second catholyte treatment (m–o)



60 spectra in order to improve the signal-to-noise ratio. A variable baseline was calculated to remove the background by applying the function “msbackadj” of the MATLAB toolboxes (MathWorks Inc., Natick, USA). This baseline was estimated within multiple windows of  $150\text{ cm}^{-1}$  width and shifted with  $150\text{ cm}^{-1}$  step and using a linear interpolation method.

Raman spectra were recorded using a Raman spectrometer RamanRxn1 (Kaiser Optical Systems Inc., Ann Arbor, USA) coupled to a light microscope DM2500 P (Leica

Microsystems GmbH, Wetzlar, Germany). The excitation of Raman scattering was obtained with a diode laser emitting at a wavelength of 785 nm, propagated to the microscope with a 100  $\mu\text{m}$  optical fiber and focused on the samples by means of a 50 $\times$ /0.75 microscope objective, leading to a focal spot of about 20  $\mu\text{m}$  with a power of 170 mW. The Raman signal was collected in reflection configuration and sent to the f/1.8 holographic imaging spectrograph by using 62.5  $\mu\text{m}$  core optical fiber. The spectral resolution in the range of 150–3250  $\text{cm}^{-1}$  was 4  $\text{cm}^{-1}$ . Raman spectra were punctually

recorded, using integration time of 1 s and averaging 60 spectra in order to improve the signal-to-noise ratio. A variable baseline was calculated to remove the background by applying the function “msbackadj” of the MATLAB toolboxes (MathWorks Inc., Natick, USA). This baseline was estimated within multiple windows of  $150\text{ cm}^{-1}$  width and shifted with  $150\text{ cm}^{-1}$  step and using a linear interpolation method.

### 2.7.7 X-ray diffraction (XRD)

The phase composition of samples was analyzed by X-ray diffraction using SEIFERT-FPM URD6 diffractometer equipped with a sealed X-ray tube with Cu anode and a secondary graphite monochromator placed in front of a proportional counter. For the measurement, the sample was fixed on its sides with scotch tape to a “zero background” to a sample holder, assuming that the amount of tape in the beam was small. The phase identification was performed with the ICDD PDF-4+ database linked to PANalytical HighScore+ software. The Rietveld refinement [73] for a more detailed analysis of the sample was conducted employing Maud software package [74].

### 2.7.8 Scanning electron microscopy (SEM)

The specimens were fixed on an aluminum sample holder with conductive carbon adhesive tabs and were sputtered with platinum for 15 s at a distance of 30 mm by an Edwards S150B sputter coater. The scanning electron micrographs were observed using a high-resolution Hitachi S-4700-II (Hitachi, Ltd., Tokyo, Japan) equipped with a cold field emission gun. The elements were analyzed by energy-dispersive X-ray spectroscopy in the EDX analysis system from EDAX and XL30ESEM Philips—scanning electron microscope (Philips, Amsterdam, the Netherlands).

## 3 Results and discussion

The main goal of this study was to develop a fast, low-cost and low-effluent method of 3D chitin isolation, based on *in situ* electrolysis of aqueous  $\text{Na}_2\text{SO}_4$  solution. The concept of electrochemically assisted isolation process was split into three main steps. Morphological changes within *A. aerophoba* sample were analyzed by digital optical microscope and SEM. Figure 7a–c shows a small cutoff of the examined sample prior to treatment in the electrolytic cell. The photographs of the sample taken right after pretreatment step (washing in distilled water) demonstrated a well-preserved original bio-architecture of *A. aerophoba* sponge (tissue structures supported by chitinous scaffold). Next, in order to decellularize the sample the electrolytic treatment was

applied (see Figs. 5, 6). Indeed, the alkaline environment of the catholyte solution should have resulted in the complete lysis of *A. aerophoba* cells. Photographic images of this process taken after 1.5 h since the beginning of the first electrochemically assisted isolation step (12 V; 0.5 A) are presented in Fig. 7d–g. The microscopic investigation of this sample revealed that cells and tissues had decomposed during catholyte treatment. Moreover, the dissolution of *A. aerophoba* somatic cells proceeded gradually from the external area of the sample to internal chitinous scaffold which is clearly visible in Fig. 7e, g. The sample cutoff after full-time catholyte treatment (3 h; 12 V; 0.5 A) is depicted in Fig. 7h–j. This image illustrates dark-brown, semitransparent and cell-free chitinous scaffold, the spatial structure of which can be characterized as typical branched network of chitinous tubes of the sponge origin. In a higher magnification, a few residues of tissue fragments can be still observed (Fig. 7j); however, the time needed to achieve this level of decomposition effect was incomparably shorter in comparison with previously reported standard methods [1, 3]. The second step of the electrochemically assisted isolation method was applied in order to remove possible carbonate salts within the sample. However, since *A. aerophoba* sponge mineralization was insignificant, this stage of the process was carried out mostly to remove acid-soluble pigments and proteins. The cutoff of the sample after full-time anolyte treatment (3 h; 12 V; 0.7 A) is presented in Fig. 7k, l. The treated sample after the second electrochemically assisted isolation step appeared in the form of a light yellow, cell-free 3D skeleton with a well preserved spatial structure consisting of branched microtubular network. The final treatment was performed to get rid of the remained proteins, pigments and possible silica remnants. Due to structural incorporation of these compounds into the chitinous tubes [21, 24], the third electrochemically assisted isolation step was conducted in extremely corrosive conditions (3 h; 16 V; 1.5 A;  $60\text{ }^\circ\text{C}$ ). Figure 7m–o shows the sample after full electrolytic treatment presented the form of a colorless scaffold with slightly harmed spatial structure of the branched tubular network. The partial damage of the spatial structure of chitinous tubes was probably caused by intensive gas evolution on the cathode. The black areas in Fig. 7m are artificial and became visible through the focus on the fibers surface. Additionally, we conducted SEM analysis (Fig. 8) of the electrochemically treated *A. aerophoba* skeleton fragments similar to those represented in Fig. 7. Corresponding EDX analysis (Fig. 8c, d) was carried out to monitor changes within the chemical composition of treated matter with respect to diverse elements usually belonging to skeletal fibers of *A. aerophoba* [21]. The nature of obtained scaffold was characterized using FTIR–ATR and XRD (see Figs. 12, 14, respectively). The identification of chitin confirmed that intensive deacetylation process and transformation of chitin into chitosan had



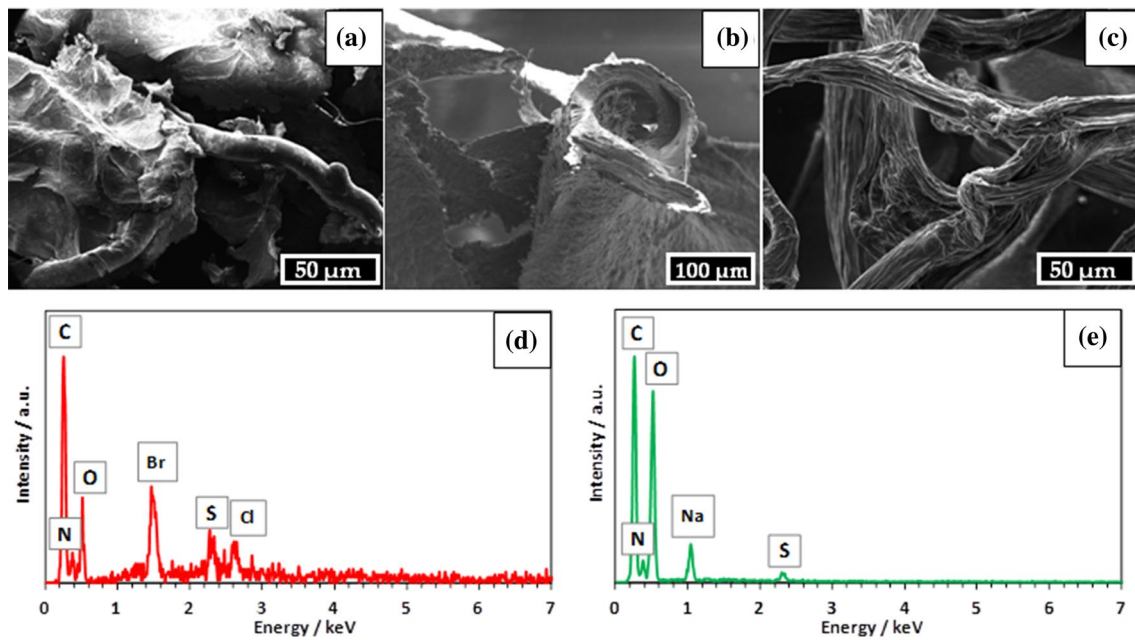


**Fig. 8** SEM imagery of the selected fragment of *A. aerophoba* sponge skeleton prior to electrolytic treatment (a) after 1.5 h of the first catholyte treatment (b) and 3 h of the second catholyte treatment (c) confirms structural changes represented in Fig. 7. EDX analysis shows changes in the chemical composition of naturally

occurring skeletal fibers (d) [corresponding to SEM image (a)] and electrochemically isolated chitinous scaffold (e) [corresponding to SEM image (c)]. Residual amounts of Na and S (e) which originated from  $\text{Na}_2\text{SO}_4$  were finally removed from chitin using dialysis against deionized water during 12 h at room temperature

not occurred under experimental conditions even after the treatment in harsh catholyte environment.

Previously, such kinds of 3D chitinous scaffolds isolated from diverse demosponges had been used in tissue engineering [1, 3, 75, 76] and extreme biomimetics [40, 77]. However, in this study we took the decision to mineralize the electrochemically isolated scaffolds of *A. aerophoba* origin using mollusk hemolymph as a unique biological system which is responsible for calcification of mechanically damaged shells in vivo.

It is well recognized that molluscan hemolymph contains calcium  $\text{Ca}^{2+}$ , bicarbonate  $\text{HCO}_3^-$  and other ions (i.e.  $\text{Na}^+$ ,  $\text{K}^+$ ,  $\text{Cl}^-$ ) [78]. Apart from these ions, molluscan hemolymph is also rich in cells and enzymes involved in  $\text{CaCO}_3$  formation such as carbonic anhydrase [79–81]. Hemocytes, primarily involved in immunoreactions, are also responsible for calcium-rich granules deposition during the formation as well as regeneration of mollusks shell [82, 83]. Eosin + methylene blue (Hemovet) is a standard stain, primarily used for the differential staining of cellular elements of blood. This protocol was used here to visualize distribution of hemocytes on the chitin scaffold [71]. Our observations made with use of eosin + methylene blue stain (see Fig. 9) clearly indicate that hemocytes react with chitin after 24 h of immersion in the hemolymph from *C. aspersum* snail. The formation of hemocyte-containing clusters (Fig. 9c) may be explained by the recognition of

chitin as a foreign body and nodulation ex vivo. Moreover, because chitin along with proteins form organic membrane during shell regeneration [84–86] hemocytes may recognize this amino polysaccharide as a natural scaffold useful for biomineralization in vivo with respect to the generation of calcium carbonates. Such chitin-containing membrane acts as a specialized scaffold for the granulocytes losing their cytoplasm full of free nuclei and organic matter and precipitating calcium-rich granules [82].

Alizarin Red S, an anthraquinone derivative, that may be used to identify calcium in tissue sections. The reaction is not strictly specific for calcium, since magnesium, manganese, barium, strontium and iron may interfere, but these elements usually do not occur in sufficient concentration to interfere with the staining. Calcium forms an Alizarin Red S–calcium complex in a chelation process, and the end product is a bright red stain. Therefore, formation of calcium-based crystals deposits on the surface of chitinous scaffold after its immersion into *C. aspersum* hemolymph could be easily confirmed by Alizarin Red S staining (see Fig. 10). Calcium deposits were detected using digital microscopy in the form of red color agglomerates tightly attached to the surface of isolated chitinous matrix. Having assumed that snail uses physical- and cellular-based processes [87–90] in shell regeneration, we aimed to analyze the polymorphs of the crystals structures obtained by biomineralization ex vivo.

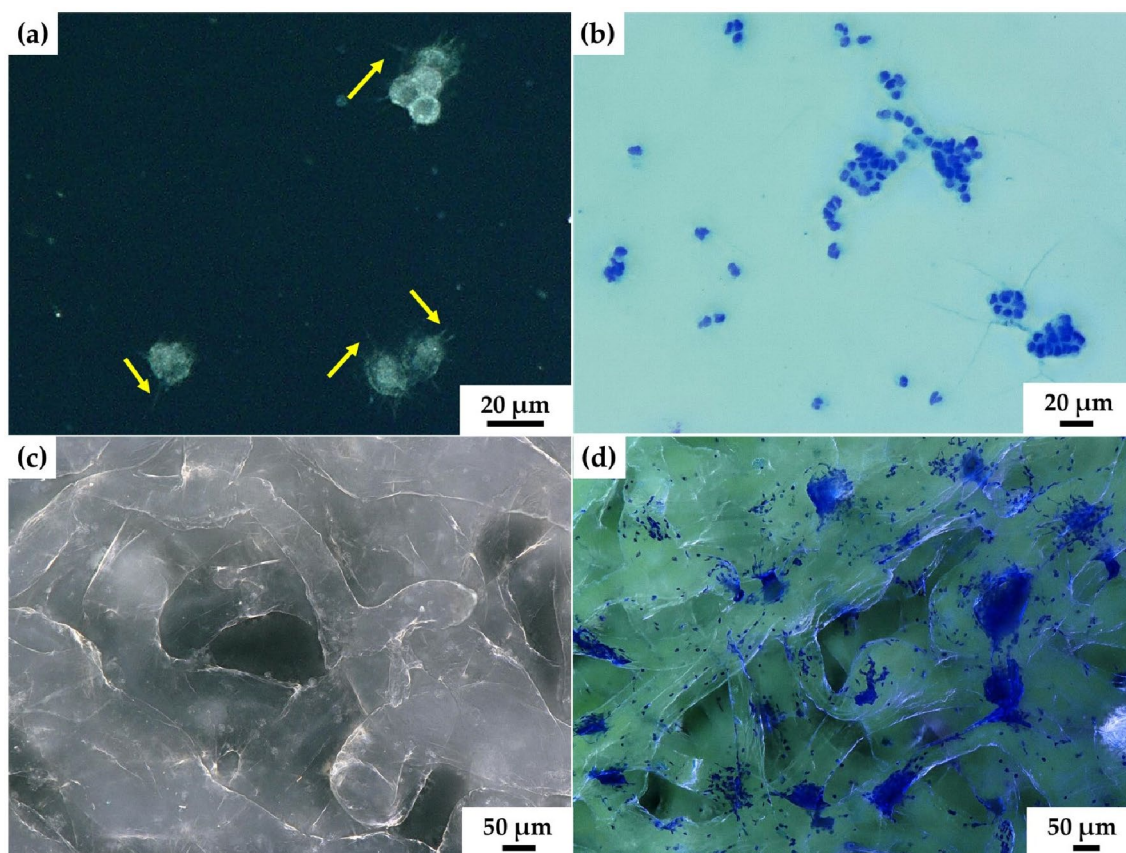


**Fig. 9** Light microscopy imagery. Single (a) and aggregated (b) hemocytes present in isolated hemolymph of *C. aspersum* snail can be observed without (a) and using eosin and methylene blue staining (b) on the glass slide. Visible pseudopodia (yellow arrows) and navy

blue color after staining indicate the presence of granulocytes (b). The formation of hemocytes-based clusters on the surface of *A. aerophoba* chitinous scaffold, after 24 h immersion in the hemolymph, prior (c) and after staining with eosin and methylene blue stain (d)

Additional analysis of the obtained deposits carried out by fluorescence microscopy indicated similarity between calcite standard [92, 93] and microgranular phase formed after biomineralization ex vivo using *C. aspersum* hemolymph with respect to the red auto-fluorescence (see Fig. 11). More advanced techniques such as ATR–FTIR (Fig. 12), Raman spectroscopy (Fig. 13) as well as X-ray diffraction analysis (Fig. 14) were further applied to identify calcium carbonate polymorph formed.

Spectra obtained using ATR–FTIR analysis of the chitinous scaffold before and after biomineralization ex vivo are demonstrated in Fig. 12. Both spectra show a characteristic band for  $\alpha$ -chitin, such as amide I at  $1633\text{ cm}^{-1}$  (see gold and grey lines). This band corresponds to the presence of stretching vibrations from intermolecular ( $\text{C}=\text{O}\cdots\text{HN}$ ) and intramolecular ( $\text{C}=\text{O}\cdots\text{HO}(\text{C}6)$ ;  $\text{C}=\text{O}\cdots\text{HN}$ ) hydrogen bonds [22, 94]. The presence of such bands as amide II ( $\nu\text{N-H}$  and  $\nu\text{C-N}$ ) at  $1548\text{--}1538\text{ cm}^{-1}$ , amide III ( $\nu\text{C-N}$  and  $\delta\text{N-H}$ ) at  $1308\text{ cm}^{-1}$  or characteristic intense bands at  $899\text{ cm}^{-1}$  ( $\text{C-O-C}$  bridge as well as glycosidic linkage) additionally proved the occurrence of  $\alpha$ -chitin in the analyzed sample. A

sharp band visible at  $873\text{ cm}^{-1}$  (see blue arrow) undeniably indicated that calcium carbonate ( $\text{CaCO}_3$ ) as monohydrocalcite polymorph [95–98] was formed at the chitinous scaffold after biomineralization.

Raman spectra acquired from the obtained crystals contain five bands (Fig. 13). Four of the five fundamental modes of calcite are visible at  $279$ ,  $710$ ,  $1083$  and  $1433\text{ cm}^{-1}$ . The first fundamental mode, normally observed at about  $155\text{ cm}^{-1}$ , lies outside the acquired spectral range. The small band at  $1746\text{ cm}^{-1}$ , which is above the highest frequency of the fundamental modes, should be attributed to an overtone of the IR active mode observed at  $873\text{ cm}^{-1}$  [99].

The results obtained using ATR–FTIR were further confirmed by XRD, being the method of choice to analyze the presence of certain crystal structures. The analysis of powder X-ray diffraction patterns of the chitinous scaffold revealed the presence of  $\text{CaCO}_3$  (calcite). Figure 14 shows a SEM micrograph of the calcium carbonate crystals, and the pattern, displayed in Fig. 14, compares the measured data with the Rietveld-like refinement of the calcite phase together with manually set background. The contributions of calcite

**Fig. 10** 3D chitinous scaffolds electrochemically isolated from *A. aerophoba* prior to biomineralization ex vivo using *C. aspersum* hemolymph are represented in digital microscopy image (a). Alizarin Red S staining of this chitin scaffold resulted in the appearance of slightly violet color (b). The formation of granular transparent calcium-based deposits on the surface of chitin after biomineralization ex vivo is well visible using digital light microscopy (c). These deposits became well visible (arrows) after Alizarin Red S staining due to intensive red coloration (d) which is indicative of Ca-based structures [91]

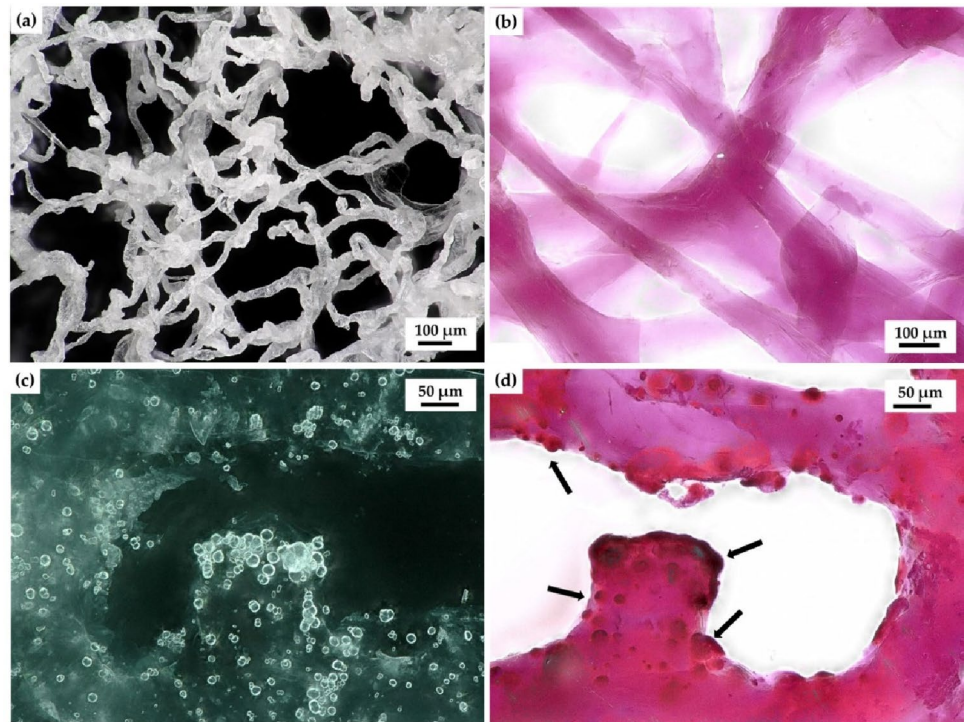
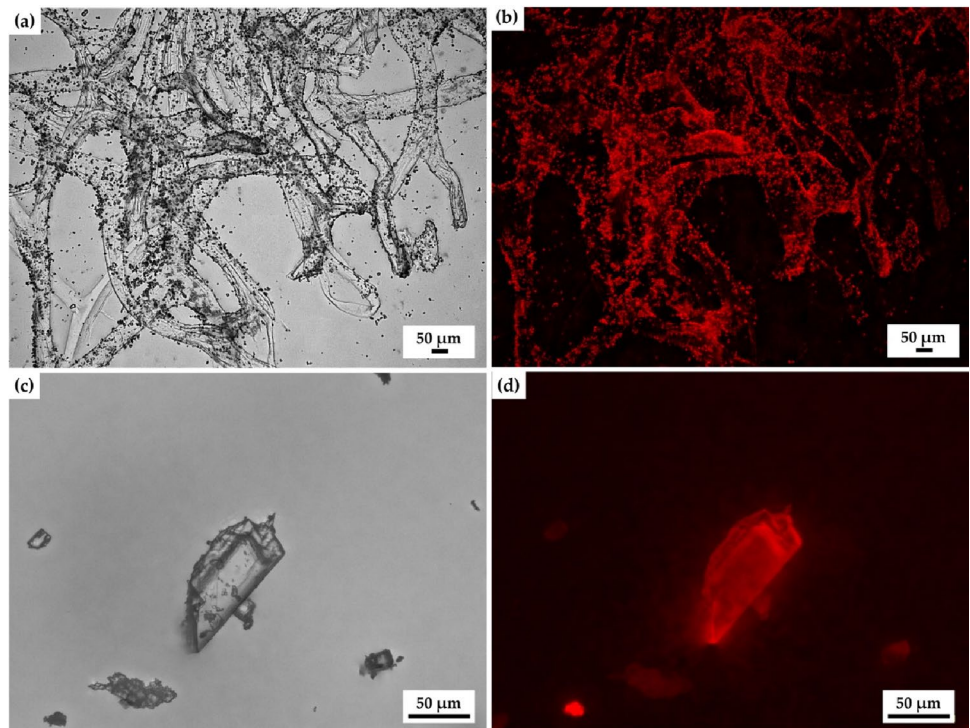


**Fig. 11** Both the mineral constituents, obtained after biomineralization ex vivo of 3D chitin scaffold (a) using hemolymph of *C. aspersum* snail as well as calcite mineral standard (c), represent a high similarity with respect to their strong red auto-fluorescence (b and d, respectively)



to the diffraction pattern are indicated at the bottom of the plot (Fig. 14) as a proof of the positive identification. The obtained lattice parameters of calcite,  $a = (4.973 \pm 0.002) \text{ \AA}$  and  $c = (16.987 \pm 0.008) \text{ \AA}$ , are smaller than the tabulated values for ambient conditions ( $a = 4.987 \text{ \AA}$ ,  $c = 17.058 \text{ \AA}$ )

[ICDD PDF #04-012-0489]. However, some maxima in the pattern could not be identified unambiguously. A large hump at  $2\theta \approx 20^\circ$  most likely corresponds to the  $\alpha$ -chitin 110 reflection [4] since chitin belongs to the scaffold as was also identified by ATR-FTIR. A second contribution to

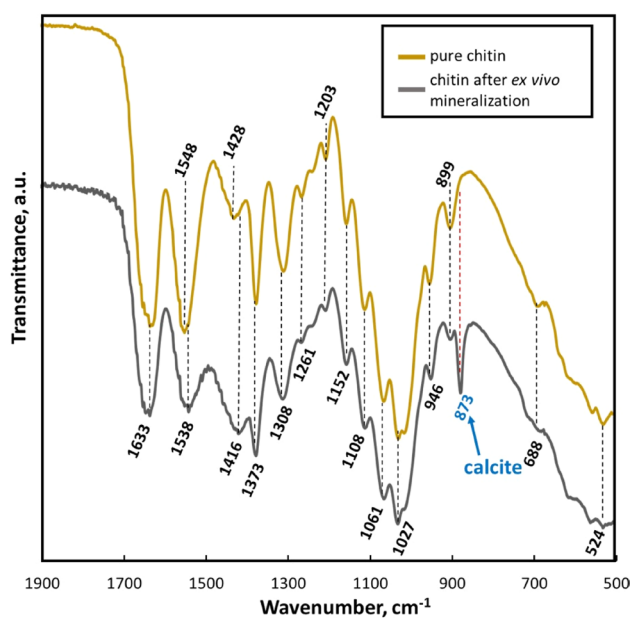


**Fig. 12** ATR-FTIR spectra of *A. aerophoba* chitin scaffold before (gold line) and after biominingalization ex vivo (grey line) in the region of 1900–500 cm<sup>-1</sup>

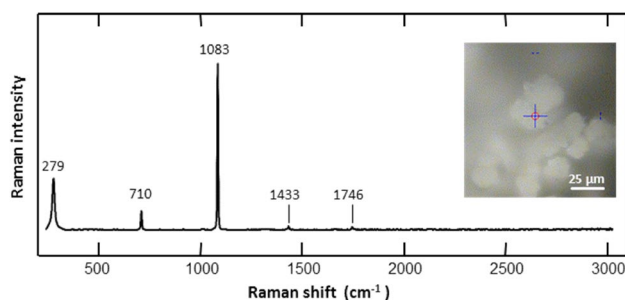


**Fig. 13** Representative graph depicting Raman spectrum of the mineral phase obtained on the surface of 3D chitinous scaffold after biominingalization ex vivo mediated by *C. aspersum* snail hemolymph

this maximum can originate from amorphous components in the samples. Other maxima at  $2\theta \approx 27^\circ$  and  $2\theta \approx 33^\circ$  must, unfortunately, remain unassigned here. The former of the two might also be explained by  $\alpha$ -chitin (102 maximum), if a preferred orientation of chitin in the scaffold is assumed. However, no in-depth analysis of this condition was undertaken.

Nowadays, data concerning practical application of calcite as well as other calcium carbonate-based phases in biomedicine and remediation in diverse environments are well represented in the literature. For example, calcium carbonate-based scaffolds have found application in modern biomedicine as constructs, which improve osteoinductive potential [100–102]. Intriguingly, natural calcium carbonate layer created by molluscs in vivo may serve as a

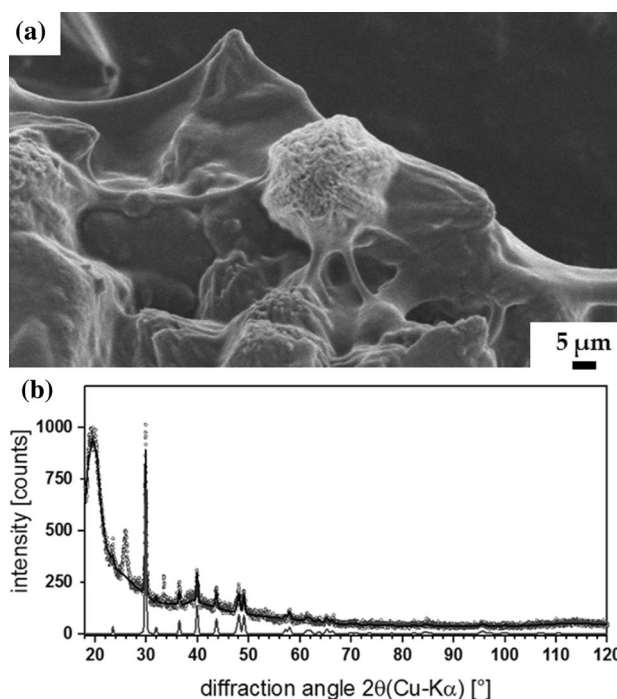


**Fig. 14** SEM micrograph of the calcium carbonate crystals (a) formed during the ex vivo biominingalization of chitinous scaffolds using hemolymph of *C. aspersum* snail Powder diffraction pattern of the chitinous scaffold after biominingalization ex vivo (b). Measured data are plotted by open dots, and the calculated intensity is highlighted by a solid line. The contribution of calcite (CaCO<sub>3</sub>) is shown at the bottom clearly verifying the presence of this phase in the sample. Two unassigned peaks remain in the data ( $2\theta \approx 27^\circ$ ,  $2\theta \approx 33^\circ$ ). The maximum at  $2\theta \approx 20^\circ$ , included in the background, belongs to the  $\alpha$ -chitin scaffold ( $\alpha$ -chitin 110 reflection) or an amorphous component in the sample

biocompatible interface between selected metals or alloys used in medical devices or as implants in human body [103].

Heavy metals present in water resources pose a high risk of hazard for human health as well as the environment. It is well recognized that calcite has a great ability to adsorb heavy metal ions [104–108]. Indeed, natural calcite as limestone [109] or in the form of waste chicken eggshells [110] has been used for heavy metal removal. In comparison with other calcium carbonate polymorphs, calcite represents the highest affinity to lead (Pb<sup>2+</sup>) [111] and cadmium (Cd<sup>2+</sup>) [112] ions. Also, a high ability of calcite for the remediation of arsenic (As) contamination from water solutions was reported [105, 106, 113]. Furthermore, in 2011, Fukushi and coworkers revealed that monohydrocalcite possesses a significantly higher arsenic sorption capacity in comparison with calcite [104]. Finally, the use of calcite as a substrate for the removal of up to 2300 mg/l fluoride from contaminated groundwater was described by Turner and coworkers [114].

Herein, for the first time we performed electrochemical isolation of natural 3D chitinous scaffolds from cultivated *A. aerophoba* marine demosponge and biomineralized them biomimetically *ex vivo* using molluscan hemolymph as a source of hemocytes and calcium. This unique method developed by us allowed the generation of crystalline (calcite) calcium carbonate-based layers, which could be useful for both biomedical and environmental applications in the future.

## 4 Conclusions

In the present work, for the first time the *in situ* electrolysis of 1.9 M Na<sub>2</sub>SO<sub>4</sub> aqueous solution in CEM membrane electrolyzer was utilized as isolation method of chitinous scaffolds from *A. aerophoba* demosponge. The final result of electrochemically assisted isolation of chitin was a colorless scaffold. The digital light microscopic investigation of this final product revealed that despite a possible mechanical damage the general spatial structure of the sample preserved its original interconnected network of unique microtubular nature. Further characterization of the isolated sample with FTIR and EDX techniques proved that a pure chitinous scaffold can be obtained by the application of described method. The perspective of the biomineralization *ex vivo* to be used in biomimetic fields which is represented in our study includes diverse open questions concerning, for example, the role of hemocytes in the generation of fine-tuned microenvironment necessary for biocalcification *ex vivo*. Without doubt, further studies on the mechanical properties of developed mineralized scaffolds aimed at practical application in environmental remediation should be carried out in the near future.

**Acknowledgements** This work was performed with the financial support of Poznan University of Technology, Poland (Grant No. 0911/SBAD/0380/2019), as well as by the Ministry of Science and Higher Education (Poland) as financial subsidy to PUT No. 03/32/SBAD/0906. Krzysztof Nowacki was supported by the Erasmus Plus program (2019). Also, this study was partially supported by the DFG Project HE 394/3 and SMWK Project No. 02010311 (Germany). Marcin Wysokowski is financially supported by the Polish National Agency for Academic Exchange (PPN/BEK/2018/1/00071). Tomasz Machałowski is supported by DAAD (Personal Ref. No. 91734605). Yuliya Khrunyk is supported by the Russian Science Foundation (Grant No. 18-13-00220).

## Compliance with ethical standards

**Conflict of interest** Authors declare no conflict of interest.

**Consent to participate** All the coworkers have agreed to participate.

**Consent for publication** All the coworkers have agreed with the publication.

**Open Access** This article is licensed under a Creative Commons Attribution 4.0 International License, which permits use, sharing, adaptation, distribution and reproduction in any medium or format, as long as you give appropriate credit to the original author(s) and the source, provide a link to the Creative Commons licence, and indicate if changes were made. The images or other third party material in this article are included in the article's Creative Commons licence, unless indicated otherwise in a credit line to the material. If material is not included in the article's Creative Commons licence and your intended use is not permitted by statutory regulation or exceeds the permitted use, you will need to obtain permission directly from the copyright holder. To view a copy of this licence, visit <http://creativecommons.org/licenses/by/4.0/>.

## References

1. V.V. Mutsenko, O. Gryshkov, L. Lauterboeck, O. Rogulska, D.N. Tarusin, V.V. Bazhenov, K. Schütz, S. Brüggemeier, E. Gossila, A.R. Akkineni, H. Meißner, A. Lode, S. Meschke, J. Fromont, A.L. Stelling, K.R. Tabachnik, M. Gelinsky, S. Nikulin, S. Rodin, A.G. Tonevitsky, Y. Petrenko, B. Glasmacher, P.J. Schupp, H. Ehrlich, *Int. J. Biol. Macromol.* **104**, 1955 (2017)
2. N. Naghshineh, K. Tahvildari, M. Nozari, *J. Polym. Environ.* **27**, 2819 (2019)
3. V.V. Mutsenko, V.V. Bazhenov, O. Rogulska, D.N. Tarusin, K. Schütz, S. Brüggemeier, E. Gossila, A.R. Akkineni, H. Meißner, A. Lode, S. Meschke, A. Ehrlich, S. Petović, R. Martinović, M. Djurović, A.L. Stelling, S. Nikulin, S. Rodin, A. Tonevitsky, M. Gelinsky, Y.A. Petrenko, B. Glasmacher, H. Ehrlich, *Int. J. Biol. Macromol.* **104**, 1966 (2017)
4. T. Machałowski, M. Wysokowski, S. Żółtowska-Aksamitowska, N. Bechmann, B. Binnewerg, M. Schubert, K. Guan, S.R. Bornstein, K. Czaczyk, O. Pokrovsky, M. Kraft, M. Bertau, C. Schimpf, D. Rafaja, M. Tsurkan, R. Galli, H. Meissner, I. Petrenko, A. Fursov, A. Voronkina, M. Figlerowicz, Y. Joseph, T. Jesionowski, H. Ehrlich, *Carbohydr. Polym.* **226**, 115301 (2019)
5. M. Norman, S. Żółtowska-Aksamitowska, A. Zgoła-Grzeszkowiak, H. Ehrlich, T. Jesionowski, *J. Hazard. Mater.* **347**, 78 (2018)
6. M. Wysokowski, T.J. Szalaty, T. Jesionowski, M. Motylenko, D. Rafaja, I. Koltsov, H. Stöcker, V.V. Bazhenov, H. Ehrlich, A.L. Stelling, J. Beyer, J. Heitmann, S. Petovic, M. Đurović, *Mater. Chem. Phys.* **188**, 115 (2017)
7. H. Ehrlich, O.V. Kaluzhnaya, E. Brunner, M.V. Tsurkan, A. Ereskovsky, M. Ilan, K.R. Tabachnik, V.V. Bazhenov, S. Paasch, M. Kammer, R. Born, A. Stelling, R. Galli, S. Belikov, O.V. Petrova, V.V. Sivkov, D. Vyalikh, S. Hunoldt, G. Wörheide, *J. Struct. Biol.* **183**, 474 (2013)
8. T. Jesionowski, M. Norman, S. Żółtowska-Aksamitowska, I. Petrenko, Y. Joseph, H. Ehrlich, *Mar. Drugs* **16**, 88 (2018)
9. T. Szatkowski, K. Koczyński, M. Motylenko, H. Borrmann, B. Mania, M. Graś, G. Lota, V.V. Bazhenov, D. Rafaja, F. Roth, J. Weise, E. Langer, M. Wysokowski, S. Żółtowska-Aksamitowska, I. Petrenko, S.L. Molodtsov, J. Hubáľková, C.G. Aneziris, Y. Joseph, A.L. Stelling, H. Ehrlich, T. Jesionowski, *Nano Res.* **11**, 4199 (2018)
10. I. Petrenko, A.P. Summers, P. Simon, S. Żółtowska-Aksamitowska, M. Motylenko, C. Schimpf, D. Rafaja, F. Roth, K. Kummer, E. Brendler, O.S. Pokrovsky, R. Galli, M. Wysokowski, H. Meissner, E. Niederschlag, Y. Joseph, S. Molodtsov, A. Ereskovsky, V. Sivkov, S. Nkepivelov, O. Petrova, O. Volkova, M. Bertau, M. Kraft, A. Rogalev, M. Kopani, T. Jesionowski, H. Ehrlich, *Sci. Adv.* **5**(10), 2805 (2019)

11. B. Duan, X. Gao, X. Yao, Y. Fang, L. Huang, J. Zhou, L. Zhang, *Nano Energy* **27**, 482 (2016)
12. H. Simsir, N. Eltugral, S. Karagoz, *Bioresour. Technol.* **246**, 82 (2017)
13. I. Stepniak, M. Galinski, K. Nowacki, M. Wysokowski, P. Jakubowska, V.V. Bazhenov, T. Leisegang, H. Ehrlich, T. Jesionowski, *RSC Adv.* **6**, 4007 (2016)
14. S. Liu, D. Li, *Appl. Surf. Sci.* **398**, 33 (2017)
15. A. Kolodziej, K. Fic, E. Frackowiak, *J. Mater. Chem. A* **3**, 22923 (2015)
16. J. Lei, J. Zhou, J. Li, J. Wen, L. Su, T. Duan, W. Zhu, *Electrochim. Acta* **285**, 292 (2018)
17. L.D. Tolesa, B.S. Gupta, M.J. Lee, *Int. J. Biol. Macromol.* **130**, 818 (2019)
18. K. Mohan, S. Ravichandran, T. Muralisankar, V. Uthayakumar, R. Chandirasekar, C. Rajeev Gandhi, D. Karthick Rajan, P. Seedeve, *Int. J. Biol. Macromol.* **126**, 555 (2019)
19. S. Liu, J. Sun, L. Yu, C. Zhang, J. Bi, F. Zhu, M. Qu, C. Jiang, Q. Yang, *Molecules* **17**, 4604 (2012)
20. M. Kaya, O. Seyyar, T. Baran, S. Erdoğan, M. Kar, *Int. J. Biol. Macromol.* **65**, 553 (2014)
21. H. Ehrlich, M. Ilan, M. Maldonado, G. Muricy, G. Bavestrello, Z. Kljajic, J.L. Carballo, S. Schiaparelli, A. Ereskovsky, P. Schupp, R. Born, H. Worch, V.V. Bazhenov, D. Kurek, V. Varlamov, D. Vyalikh, K. Kummer, V. Sivkov, S.L. Molodtsov, H. Meissner, G. Richter, E. Steck, W. Richter, S. Hunoldt, M. Kammer, S. Paasch, V. Krasokhin, G. Patzke, E. Brunner, *Int. J. Biol. Macromol.* **47**, 132 (2010)
22. M. Kaya, M. Mujtaba, H. Ehrlich, A.M. Salaberria, T. Baran, C.T. Amemiya, R. Galli, L. Akyuz, I. Sargin, J. Labidi, *Carbohydr. Polym.* **176**, 177 (2017)
23. M. Rinaudo, *Prog. Polym. Sci.* **31**, 603 (2006)
24. H. Ehrlich, *Int. Geol. Rev.* **52**, 661 (2010)
25. H. El Knidri, R. Belaabed, A. Addaou, A. Laajeb, A. Lahsini, *Int. J. Biol. Macromol.* **120**, 1181 (2018)
26. T. Philibert, B.H. Lee, N. Fabien, *Appl. Biochem. Biotechnol.* **181**, 1314 (2017)
27. C.Y. Soon, Y.B. Tee, C.H. Tan, A.T. Rosnita, A. Khalina, *Int. J. Biol. Macromol.* **108**, 135 (2018)
28. I. Younes, M. Rinaudo, *Mar. Drugs* **13**, 1133 (2015)
29. H. Ehrlich, L.A. Shaala, D.T.A. Youssef, S. Żółtowska-Aksamitowska, M. Tsurkan, R. Galli, H. Meissner, M. Wysokowski, I. Petrenko, K.R. Tabachnick, V.N. Ivanenko, N. Bechmann, Y. Joseph, T. Jesionowski, *PLoS ONE* **13**, e0195803 (2018)
30. A. Percot, C. Viton, A. Domard, *Biomacromol.* **4**, 12 (2003)
31. Y. Dun, Y. Li, J. Xu, Y. Hu, C. Zhang, Y. Liang, S. Zhao, *Int. J. Biol. Macromol.* **123**, 420 (2019)
32. Y. Kim, R.D. Park, *J. Korean Soc. Appl. Biol. Chem.* **58**, 545 (2015)
33. M.C. Gortari, R.A. Hours, *Electron. J. Biotechnol.* **16**, 14 (2013)
34. A. Khanafari, R. Marandi, S. Sanatei, *Iran J. Environ. Health Sci. Eng.* **5**, 1 (2008)
35. H. El Knidri, J. Dahmani, A. Addaou, A. Laajeb, A. Lahsini, *Int. J. Biol. Macromol.* **139**, 1092 (2019)
36. E.E. Kuprina, G.V. Maslova, E.V. Bachische, in: *IXth International Conference: Modern Perspectives in Chitin and Chitosan Studies* (Stavropol, Russia, 2008), pp. 30–33
37. M. Feng, X. Lu, J. Zhang, Y. Li, C. Shi, L. Lu, S. Zhang, *Green Chem.* **21**, 87 (2019)
38. H. Ehrlich, M. Maldonado, K. Spindler, C. Eckert, T. Hanke, R. Born, C. Goebel, P. Simon, S. Heinemann, H. Worch, *J. Exp. Zool. Part B Mol. Dev. Evol.* **308B**, 347 (2007)
39. E. Brunner, H. Ehrlich, P. Schupp, R. Hedrich, S. Hunoldt, M. Kammer, S. Machill, S. Paasch, V.V. Bazhenov, D.V. Kurek, T. Arnold, S. Brockmann, M. Ruhnnow, R. Born, *J. Struct. Biol.* **168**, 539 (2009)
40. M. Wysokowski, I. Petrenko, A.L. Stelling, D. Stawski, T. Jesionowski, H. Ehrlich, *Polymers* **7**, 235 (2015)
41. M. Wysokowski, V.V. Bazhenov, M.V. Tsurkan, R. Galli, A.L. Stelling, H. Stöcker, S. Kaiser, E. Niederschlag, G. Gärtner, T. Behm, M. Ilan, A.Y. Petrenko, T. Jesionowski, H. Ehrlich, *Int. J. Biol. Macromol.* **62**, 94 (2013)
42. H. Ehrlich, V.V. Bazhenov, C. Debitus, N. de Voogd, R. Galli, M.V. Tsurkan, M. Wysokowski, H. Meissner, E. Bulut, M. Kaya, T. Jesionowski, *Int. J. Biol. Macromol.* **104**, 1706 (2017)
43. C. Klinger, S. Żółtowska-Aksamitowska, M. Wysokowski, M.V. Tsurkan, R. Galli, I. Petrenko, T. Machałowski, A. Ereskovsky, R. Martinović, L. Muzychka, O.B. Smolii, N. Bechmann, V. Ivanenko, P.J. Schupp, T. Jesionowski, M. Giovine, Y. Joseph, S.R. Bornstein, A. Voronkina, H. Ehrlich, *Mar. Drugs* **17**, 131 (2019)
44. T. Machałowski, M. Wysokowski, M.V. Tsurkan, R. Galli, C. Schimpf, D. Rafaja, E. Brendler, C. Viehweger, S. Żółtowska-Aksamitowska, I. Petrenko, K. Czaczyk, M. Kraft, M. Bertau, N. Bechmann, K. Guan, S.R. Bornstein, A. Voronkina, A. Fursov, M. Bejger, K. Biniek-Antosiak, W. Rypniewski, M. Figlerowicz, O. Pokrovsky, T. Jesionowski, H. Ehrlich, *Molecules* **24**, 3736 (2019)
45. E.E. Kuprina, K.G. Timofeeva, E.V. Krasavtsev, A. Boykov, in: *VIIIth International Conference: Modern Perspectives in Chitin and Chitosan Studies* (Kazan, Russia, 2006), pp. 34–37
46. E.E. Kuprina, K.G. Timofeeva, I. Kozlova, A. Pimenov, in: *VIIth International Conference: Modern Perspectives in Chitin and Chitosan Studies* (St. Petersburg-Repino, Russia, 2003), pp. 19–21
47. E.E. Kuprina, S.V. Vodolazhskaya, G.G. Nyanikova, K.G. Timofeeva, in: *VIth International Conference: New Achievements in Study of Chitin and Chitosan* (Moscow, Shchelkovo, Russia, 2001), pp. 31–34
48. E.E. Kuprina, V. Krasavtsev, I. Kozlova, S. Vodolazhskaya, A. Bogeruk, in: *Vth International Conference: New Prospects in Study of Chitin and Chitosan* (Moscow, Shchelkovo, Russia, 1999), pp. 42–44
49. E.E. Kuprina, K.G. Timofeeva, S.V. Vodolazhskaya, *Russ. J. Appl. Chem.* **75**, 822 (2002)
50. A.T. Gladstone, *J. Chem. Soc.* **30**, 152 (1876)
51. H.V. Atwell, T. Fuwa, *Ind. Eng. Chem.* **15**, 617 (1923)
52. K. Tennakone, *Int. J. Hydrogen Energy* **14**, 681 (1989)
53. G.G. Scherer, T. Momose, K. Tomiie, *J. Electrochem. Soc.* **135**, 3071 (1988)
54. S. Haddadi, G.R. Nabi-Bidhendi, N. Mehrdadi, *J. Environ. Health Sci. Eng.* **12**, 48 (2014)
55. M. Zeppilli, A. Lai, M. Villano, M. Majone, *Chem. Eng. J.* **304**, 10 (2016)
56. A.K. Das, M. Manohar, V.K. Shahi, *J. Memb. Sci.* **552**, 377 (2018)
57. L.A. Diaz, T.E. Lister, C. Rae, N.D. Wood, A.C.S. Sustain, *Chem. Eng.* **6**, 8458 (2018)
58. X. Li, X. Jin, N. Zhao, I. Angelidaki, Y. Zhang, *Water Res.* **119**, 67 (2017)
59. D.A. Salvatore, D.M. Weekes, J. He, K.E. Dettelbach, Y.C. Li, T.E. Mallouk, C.P. Berlinguette, *ACS Energy Lett.* **3**, 149 (2018)
60. B. Pisarska, I. Wicher, R. Dylewski, *Przem. Chem.* **83**, 186 (2004)
61. S. Holze, J. Jörissen, C. Fischer, H. Kalvelage, *Chem. Eng. Technol.* **17**, 382 (1994)
62. J. Jörissen, K.H. Simmrock, *J. Appl. Electrochem.* **21**, 869 (1991)
63. B. Binnewerg, M. Schubert, A. Voronkina, L. Muzychka, M. Wysokowski, I. Petrenko, M. Djurović, V. Kovalchuk, M.

- Tsurkan, R. Martinovic, N. Bechmann, A. Fursov, V.N. Ivanenko, K.R. Tabachnick, O.B. Smolii, Y. Joseph, M. Giovine, S.R. Bornstein, A.L. Stelling, A. Tunger, M. Schmitz, O.S. Taniya, I.S. Kovalev, G.V. Zyryanov, K. Guan, H. Ehrlich, *Mater. Sci. Eng. C* **109**, 110566 (2020)
64. J. Ziętek, L. Guz, K. Panasiuk, S. Winiarczyk, Ł. Adaszek, *Med. Weter.* **73**, 366 (2017)
65. J. Ziętek, L. Guz, S. Winiarczyk, K. Szkucik, M. Ziomek, M. Wysokowski, J. Madany, L. Adaszek, *Pol. J. Vet. Sci.* **21**, 445 (2018)
66. A. Abolins-Krogis, *Symp. Zool. Soc. London* **22**, 75 (1968)
67. A. De Waele, *Bull. l'Académie R des Sci Belgique Cl des Sci* **10**, 1 (1930)
68. A.S.M. Saleuddin, W. Chan, *Can. J. Zool.* **47**, 1107 (1969)
69. J.-M. Lebel, W. Giard, P. Favrel, E. Boucaud-Camou, *Biol. Cell* **86**, 67 (1996)
70. L. Donaghy, H.K. Hong, C. Lambert, H.S. Park, W.J. Shim, K.S. Choi, *Fish Shellfish Immunol.* **28**, 87 (2010)
71. R. Grandiosa, F. Mérien, K. Pillay, A. Alfaro, *Fish Shellfish Immunol.* **48**, 175 (2016)
72. S. Li, Y. Liu, C. Liu, J. Huang, G. Zheng, L. Xie, R. Zhang, *Fish Shellfish Immunol.* **51**, 263 (2016)
73. H.M. Rietveld, *Acta Crystallogr.* **22**, 151 (1967)
74. L. Lutterotti, S. Matthies, H. Wenk, *Comm. Power Differ. Newsl.* **21**, 1 (1999)
75. V. Mutsenko, A. Barlič, T. Pezić, J. Dermol-Černe, B. Dovgan, B. Sydykov, W.F. Wolkers, I.I. Katkov, B. Glasmacher, D. Miklavčič, O. Gryshkov, *Cryobiology* **91**, 104 (2019)
76. M. Schubert, B. Binnewerg, A. Voronkina, L. Muzychka, M. Wysokowski, I. Petrenko, V. Kovalchuk, M. Tsurkan, R. Martinovic, N. Bechmann, V.N. Ivanenko, A. Fursov, O.B. Smolii, J. Fromont, Y. Joseph, S.R. Bornstein, M. Giovine, D. Erpenbeck, K. Guan, H. Ehrlich, *Int. J. Mol. Sci.* **20**, 5105 (2019)
77. M. Wysokowski, M. Motylenko, J. Beyer, A. Makarova, H. Stöcker, J. Walter, R. Galli, S. Kaiser, D. Vyalikh, V.V. Bazhenov, I. Petrenko, A.L. Stelling, S.L. Molodtsov, D. Stawski, K.J. Kurzydłowski, E. Langer, M.V. Tsurkan, T. Jesionowski, J. Heitmann, D.C. Meyer, H. Ehrlich, *Nano Res.* **8**, 2288 (2015)
78. L. Deatton, in: *Osmotic and Ionic Regulation: Cells and Animals* ed. by D.H. Evans (CRC Press, New York, 2008), pp. 107–125
79. R.P. Henry, D.G. Saintsing, *Physiol. Zool.* **56**, 274 (1983)
80. S. Auzoux-Bordenave, M. Fouchereau-Peron, M.N. Helleouet, D. Doumenc, *J. Shellfish Res.* **26**, 887 (2007)
81. A.P. Wheeler, in: *The Calcification in Biological System* ed. by E. Bonucci (CRC Press, London, 1992), pp. 179–210
82. S.P. Kapur, A. Sen Gupta, *Biol. Bull.* **139**, 502 (1970)
83. A. Abolins-Krogis, *Cell Tissue Res.* **172**, 455 (1976)
84. L. Addadi, D. Joester, F. Nudelman, S. Weiner, *Chem.: A Eur. J.* **12**, 980 (2006)
85. X. Du, G. Fan, Y. Jiao, H. Zhang, X. Guo, R. Huang, Z. Zheng, C. Bian, Y. Deng, Q. Wang, Z. Wang, X. Liang, H. Liang, C. Shi, X. Zhao, F. Sun, R. Hao, J. Bai, J. Liu, W. Chen, J. Liang, W. Liu, Z. Xu, Q. Shi, X. Xu, G. Zhang, X. Liu, *Gigascience* **6**, 1 (2017)
86. V.B.S. Chan, M.B. Johnstone, A.P. Wheeler, A.S. Mount, *Front. Mar. Sci.* **5**, 347 (2018)
87. A. Abolins-Krogis, *Zeitschrift für Zellforschung und mikroskopische Anat* **142**, 205 (1973)
88. J. Huang, S. Li, Y. Liu, C. Liu, L. Xie, R. Zhang, *Sci. Rep.* **8**, 4657 (2018)
89. A.S. Mount, A.P. Wheeler, R.P. Paradkar, D. Snider, *Science* **304**, 297 (2004)
90. A.S. Mount, N.V. Gohad, D.C. Hansen, K.M. Hansen, M. Beth, M.B. Johnstone, US 9,371,451 B2 (2016)
91. M. Li, Y. Wu, Y. Zhang, H. Xia, Y. Zheng, Y. Han, *Sci. Rep.* **6**, 32323 (2016)
92. P.J. Modreski, R. Aumente-Modreski, *Rocks Miner. Mag.* **71**, 14 (1996)
93. J. DeMent, *Handbook of Fluorescent Gems and Minerals: An Exposition and Catalog of the Fluorescent and Phosphorescent Gems and Minerals, Including the Use of Ultraviolet Light in the Earth Sciences* (Brunauer Press, London, 2014)
94. J. Kumirska, M. Czerwicka, Z. Kaczyński, A. Bychowska, K. Brzozowski, J. Thöming, P. Stepnowski, *Mar. Drugs* **8**, 1567 (2010)
95. F.B. Reig, J.V.G. Adelantado, M.C.M. Moya Moreno, *Talanta* **58**, 811 (2002)
96. L.C. Prinsloo, *J. Raman Spectrosc.* **38**, 496 (2007)
97. M. Señorale-Pose, C. Chalar, Y. Dauphin, P. Massard, P. Pradel, M. Marín, *Exp. Parasitol.* **118**, 54 (2008)
98. E.E. Coleyshaw, G. Crump, W.P. Griffith, *Spectrochim. Acta A Mol. Biomol. Spectrosc.* **59**, 2231 (2003)
99. M.D. Pierre, C. Carteret, L. Maschio, E. André, R. Orlando, R. Dovesi, *J. Chem. Phys.* **140**, 164509 (2014)
100. H. Bahrom, A.A. Goncharenko, L.I. Fatkhutdinova, O.O. Peltek, A.R. Muslimov, O.Y. Koval, I.E. Eliseev, A. Manchev, D. Gorin, I.I. Shishkin, R.E. Noskov, A.S. Timin, P. Ginzburg, M.V. Zyzin, A.C.S. Sustain, *Chem. Eng. J.* **7**, 19142 (2019)
101. B. Kruppke, J. Farack, S. Weil, E.D. Aflalo, D. Polakova, A. Sagi, T. Hanke, *J. Biomed. Mater. Res. Part A* **108**, 694 (2019)
102. E. Tolba, W.E.G. Müller, B.M. Abd El-Hady, M. Neufurth, F. Wurm, S. Wang, H.C. Schröder, X. Wang, *J. Mater. Chem. B* **4**, 376 (2016)
103. A.S. Mount, N.V. Gohad, D.C. Hansen, K. Muller, M.B. Johnstone, US 8,541,031 B2 (2013)
104. K. Fukushi, T. Munemoto, M. Sakai, S. Yagi, *Sci. Technol. Adv. Mater.* **12**, 064702 (2011)
105. S. Goldberg, R.A. Glaubig, *Soil Sci. Soc. Am. J.* **52**, 1297 (1988)
106. S. Song, A. Lopez-Valdivieso, D.J. Hernandez-Campos, C. Peng, M.G. Monroy-Fernandez, I. Razo-Soto, *Water Res.* **40**, 364 (2006)
107. T. Yang, R. He, G. Nie, W. Wang, G. Zhang, Y. Hu, L. Wu, *Sci. Rep.* **8**, 17603 (2018)
108. Ö. Yavuz, R. Guzel, F. Aydin, I. Tegin, R. Ziyadanogullari, *Polish. J. Environ. Stud.* **16**, 467 (2007)
109. A. Sdiri, T. Higashi, *Appl. Water Sci.* **3**, 29 (2013)
110. M.S. Tizo, A.L.V. Blanco, A.C.Q. Cagas, B.R.B. Dela Cruz, J.C. Encoy, J.V. Gunting, R.O. Arazo, I.V.F. Mabayo, *Sustain Environ. Res.* **28**, 326 (2018)
111. F. Di Lorenzo, C. Ruiz-Agudo, S.V. Churakov, *Cryst. Eng. Commun.* **21**, 6145 (2019)
112. O.L. Gaskova, M.B. Bukaty, G.P. Shironosova, V.G. Kabannik, *Russ. Geol. Geophys.* **50**, 87 (2009)
113. Y. Yokoyama, T. Iwatsuki, Y. Terada, Y. Takahashi, *J. Phys. Conf. Ser. Relat.* **430**, 012099 (2013)
114. B.D. Turner, P.J. Binning, S.W. Sloan, *J. Contam. Hydrol.* **95**, 110 (2008)

**Publisher's Note** Springer Nature remains neutral with regard to jurisdictional claims in published maps and institutional affiliations.

## Affiliations

Krzysztof Nowacki<sup>1</sup> · Izabela Stępnia<sup>1</sup> · Tomasz Machałowski<sup>2,3</sup> · Marcin Wysokowski<sup>2,3</sup> · Iaroslav Petrenko<sup>3</sup> · Christoph Schimpf<sup>4</sup> · David Rafaja<sup>4</sup> · Enrico Langer<sup>5</sup> · Andreas Richter<sup>5</sup> · Jerzy Ziętek<sup>6</sup> · Snežana Pantović<sup>7</sup> · Alona Voronkina<sup>8</sup> · Valentine Kovalchuk<sup>9</sup> · Viatcheslav Ivanenko<sup>10,11</sup> · Yuliya Khrunyk<sup>12,13</sup> · Roberta Galli<sup>14</sup> · Yvonne Joseph<sup>3</sup> · Michael Gelinsky<sup>15</sup> · Teofil Jesionowski<sup>2</sup> · Hermann Ehrlich<sup>3,16</sup>

<sup>1</sup> Institute of Chemistry and Technical Electrochemistry, Poznan University of Technology, ul. Berdychowo 4, 60-965 Poznan, Poland

<sup>2</sup> Institute of Chemical Technology and Engineering, Faculty of Chemical Technology, Poznan University of Technology, Berdychowo 4, 60965 Poznan, Poland

<sup>3</sup> Institute of Electronics and Sensor Materials, TU Bergakademie Freiberg, Gustav-Zeuner Str. 3, 09599 Freiberg, Germany

<sup>4</sup> Institute of Materials Science, TU Bergakademie Freiberg, 09599 Freiberg, Germany

<sup>5</sup> Institute of Semiconductors and Microsystems, TU Dresden, 01062 Dresden, Germany

<sup>6</sup> Department of Epizootiology and Clinic of Infectious Diseases, Faculty of Veterinary Medicine, University of Life Sciences, Głęboka 30, 20612 Lublin, Poland

<sup>7</sup> Faculty of Medicine, University of Montenegro, Kruševac bb, 81000 Podgorica, Montenegro

<sup>8</sup> Department of Pharmacy, National Pirogov Memorial Medical University, Vinnytsia 21018, Ukraine

<sup>9</sup> Department of Microbiology, National Pirogov Memorial Medical University, Vinnytsya, Vinnytsia 21018, Ukraine

<sup>10</sup> Department of Invertebrate Zoology, Biological Faculty, Lomonosov Moscow State University, Moscow, Russia 119992

<sup>11</sup> Taxonomy and Systematics Group, Naturalis Biodiversity Center, 2300 RA Leiden, The Netherlands

<sup>12</sup> Ural Federal University, Mira Str. 19, Ekaterinburg, Russia 620002

<sup>13</sup> The Institute of High Temperature Electrochemistry, Ural Branch of the Russian Academy of Sciences, Akademicheskaya Str. 20, Ekaterinburg, Russia 620990

<sup>14</sup> Clinical Sensing and Monitoring, Department of Anesthesiology and Intensive Care Medicine, Faculty of Medicine, TU Dresden, 01307 Dresden, Germany

<sup>15</sup> Centre for Translational Bone, Joint, Soft Tissue Research, Medical Faculty and University Centre for Orthopaedics and Trauma Surgery, University Hospital Carl Gustav Carus at Technische Universität Dresden, 01307 Dresden, Germany

<sup>16</sup> Center for Advanced Technology, Adam Mickiewicz University, 61614 Poznan, Poland